Surface & Coatings Technology 464 (2023) 129556

Contents lists available at ScienceDirect

Surface & Coatings Technology

journal homepage: www.elsevier.com/locate/surfcoat

Multilayered WC–Co coatings by Direct Energy Deposition-based cladding: Effect of laser remelting on interface defects

Erica Liverani *, Alessandro Ascari, Alessandro Fortunato

Department of Industrial Engineering (DIN), University of Bologna, viale Risorgimento 2, Bologna, Italy

ARTICLE INFO

Keywords:
Direct Energy Deposition
DED-based cladding
WC-Co
Remelting
Multilayer deposition

ABSTRACT

Despite ongoing optimization of WC-Co Direct Energy Deposition-based cladding, the deposition of multilayer coating is currently challenging. Pores and cracks that extended along the deposit thickness have been always observed in medium-large multilayer coatings. The change of substrate from steel to hard metal in multilayer deposition, replaces all of the thermal characteristics and dilution modes. This study looks into ways to improve the deposition quality of WC-Co multilayers for metal cutting application by remelting between subsequent layers. In order to define the key process parameters and to identify the effects of remelting, the characteristics of coatings are first examined in a single-track and single-layer simplified condition. These initial tests demonstrate that remelting reduces porosity and identify a "white layer" microstructural modification. The multilayer configuration was then examined, and a thorough analysis of the microstructure revealed an enrichment in Fe-Co-C elements in the surface that was advantageous for the deposition of a second layer. Remelting's observed effects on porosity and microstructure have been discussed, and the method's advantages and drawbacks have been made clear for potential future application.

1. Introduction

In the last three decades, metal and ceramic powders have been deposited on metal substrates using laser technology as a heat source with the aim of finding an alternative coating approach to plasma, thermal spray or arc welding deposition. Laser cladding is the process used for adding coating to the surface of metal components while Direct Energy Deposition (DED) is an Additive Manufacturing process evolved from cladding by implementing a robotic multilayer deposition for bulk components production. When implemented as a cladding technique, DED includes feeding wire or powder into a melt pool generated by the laser beam as it sweeps across the component surface to be covered. Coatings are usually deposited in order to improve wear or corrosion performance of surface starting from less resistant metallic substrates and require homogeneous properties and low defects. The DED-based cladding has several benefits over other coating techniques [1,2], including a stronger metallurgical bond between the substrate and the coating material; a minimization of strains and distortions within the deposited materials by providing a regulated low heat input with less dilution and Heat Affected Zone (HAZ) and a production of finer microstructures due to the rapid cooling rate that result is higher mechanical strength of coating. Furthermore, a broad range of alloys and composites are compatible with this process and the same equipment is required for all cases. In the last years, the potential of this technology pushed interest further with several studies devoted to metallurgy, with a particular focus on ceramic [3,4] and composite materials as Metal Matrix Composites (MMCs) [5,6], process monitoring [7,8] and modeling [9,10].

The resulting mechanical properties and microstructure of coatings produced by DED-based cladding were extensively studied in particular in case of metal deposition and the effect of process parameters correlate to each other's.

Ceramic coatings, however, are subjected to crack initiation and propagation that occurs due the thermal stress caused by the difference of thermal expansion coefficient between the ceramic and substrate metallic materials [11]. This issue is even more pronounced for WC ceramic-metal composite coating owing to their very different thermophysical properties with metal matrix. Several authors explore the crack forming mechanism of WC ceramic-metal composite coatings.

Zhou et al. [12] identified two different directions of crack propagation: longitudinal cracks at the interface of the composite coating and the substrate and transversal cracks, which was perpendicular to the

* Corresponding author.
E-mail address: erica.liverani2@unibo.it (E. Liverani).

https://doi.org/10.1016/j.surfcoat.2023.129556
Received 9 February 2023; Received in revised form 6 April 2023; Accepted 19 April 2023
Available online 25 April 2023

laser scanning direction. With a particular attention to transversal cracks Liu et al. [13] highlight two mechanisms for crack formation; a WC particle cracking and WC/W2C interface decohesion. When the thermal stress between the WC and matrix was greater than the WC's yield strength, cracks would start inside WC particles and propagate along eutectic phases. The crack susceptibility increases with stress concentration and this is favored from high wt% of WC that results in higher amount of carbide precipitates [14]. In literature there are many works that aim to prevent cracks of WC ceramic-metal coating, including process parameters optimization [15], correct weight percentage of ceramic phases definition [16], appropriate WC-doping [17], preheating substrate [18], etc. As a result, crack-free composite coating could be obtained by selecting appropriate process parameters, although minor defects occur as porosities or microstructural inhomogeneity. Promising results were presented also in case of multi-layer, single-track deposition. Xiong et al. [19] obtain crack-free thin wall deposition by using low-speed process parameters, in particular in terms of height increment and laser speed. Balla et al. [20] obtain similar results (porosity less than 2 %) also at higher speed and deposition rate.

The circumstances of deposition are radically different when switching from a one-layer coating or multi-track coating to a multilayer coating since the substrate changes for the n-layers from metal to hard metal and adjacent passes prevent optimal heat dissipation, along with all of the thermal characteristics and dilution modes.

Pores, uneven reaction zones, and cracks that extended along the depth direction were observed in multilayer coatings by Wang et al. [21], unlike what was analyzed between the substrate and the first layer. For solving this cracking tendency Wang et al. [22] used a C276 alloy as the first layer for reducing the hardness difference between the substrate and the gradient coating. However, when an interlayer is not allowed other manufacturing strategies need to be implemented.

The approach proposed in this paper involves the surface remelting of the first layer to improve the deposition of a second layer. According to Yu et al. [23] laser remelting eliminates the un-melted powders stuck to the surface of the first layer improving surface roughness and reducing interlayer and intralayer porosity. Additionally, the laser remelting procedure modifies the sample's thermal history and consequently the relation between the volume faction of precipitates and microstructural homogeneity [23]. Mateos et al. [24] and Afzal et al. [25] used laser remelting strategy after plasma-sprayed coating and demonstrate an improvement of dry wear resistance.

To the best of the authors' knowledge, no papers have deeply investigated the effect of WC-Co layer cladded remelting for improving the multi-track and multi-layer deposition of medium-large areas (square centimeters of deposited areas). In this regard, the proposed paper focuses on assessing the remelting interaction between laser and WC-Co and evaluates the impact of further deposition in terms of defects as porosity and cracking.

The experimental campaign began with the assessment of the first layer's quality as DED-based cladding process parameters varied, went on to analyze the effects of remelting on the variation of the process parameters, and concluded with the assessment of this method's influence on the deposition of a second layer. All under single- and multiple-track circumstances.

2. Material and methods

2.1. Sample manufacturing

The DED cladding system used for the experiments is based on a 6 axes ABB IRB 4600 robot and a 2 axes IRBP A250 external roto-tilting positioner. The laser source is a Laserline LDF-4500-60 diode one equipped by a feeding fiber with a 600 μm core diameter. The focusing optics is a Laserline OTS-5 with a collimating focal length of 80 mm and a focalization focal length of 300 mm: this configuration gives a final spot on the workpiece with a diameter of 2.2 mm. The powder nozzle is a 6-ways GTV PN6625 with a standoff distance of 25 mm and a powder jet focus of approximately 2 mm, while the powder feeder is a GTV PS2/2. The cladding optics is equipped by the NIT Clamir monitoring system that allows a closed loop control of the laser power in order to keep the melt pool dimension constant during the deposition process.

Table 1
Nominal WC-Co powder chemical composition [wt%].

W	*Co*	*C*	*Fe*
Balance	11.94	5.49	0.022

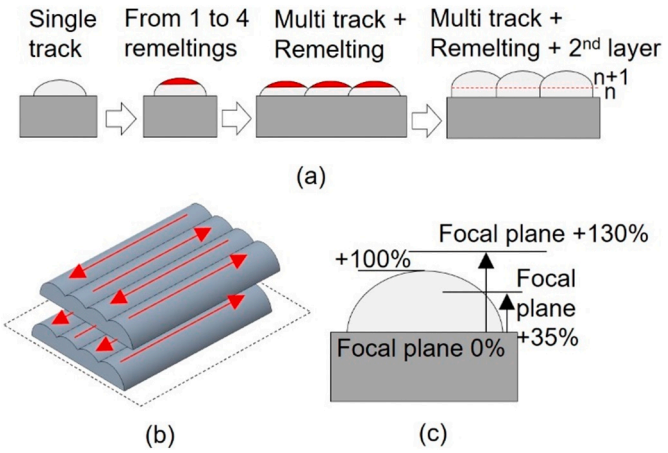

Fig. 1. Laboratory-based 4 stages experiments (a), scan direction for multitrack and multilayer deposition (b) and remelting focal place position (c).

WC-12Co atomized powder, supplied by GTV (GTV Verschleißschutz GmbH, Luckenbach, Germany), with the chemical composition reported in Table 1 was used for the experimental campaign. The powder had a particle size 53 μm ± 15 μm and were deposited on Fe bulk substrate. Argon was used as carrier and shielding gas with a flow rate of 7.5 l/min.

Four step laboratory-based experiments were scheduled as shown in Fig. 1a: (1) Single track process parameters evaluation, (2) metallurgical effect of post-remelting and analysis of number of re-melting outcomes in a single-track configuration and (3) multitrack configuration, (4) results of re-melting method on the quality of a second layer deposition (in a multitrack configuration).

In steps three and four, where multitrack setup was defined, the deposition strategy is bidirectional with laser on from both extremes of tracks and hatch distance between adjacent track of 1.3 mm. In case of double layer, the deposition occurs by overlapping scanning strategy (see Fig. 1b).

Although the preliminary experimental campaign that defined the reference process parameters for single track deposition is not discussed in this paper, the tested conditions and relevant findings are summarized below:

- Powers between 500 and 1500 W, laser speeds between 6 and 12 mm/s, and powder feed rates between 4 and 20 g/min were assessed.
- Material shortages result from powder feed rates of 4 to 10 g/min combined with speeds of 6 to 12 mm/s (considered acceptable in terms of productivity), whereas feed rates of 12 to 15 g/min prevent a sufficient dilution of the layer on the substrate.
- Dilution from 15 to 35 % was measured while keeping the feed rate fixed at 11.6 g/min (= 2.5 RPM).
- In the tested range, the track's morphology does not vary greatly in terms of height (max 20 %), but speeds below 10 mm/s cause an evident increase in porosity.

Table 2
Reference process parameters for single track's deposition.

	Power [W]	Scan speed [mm/s]	Irradiance [W/cm^2]
REF1	1300	8	3.42×10^4
REF2	900	8	2.37×10^4

- Speeds of 6 mm/s or lower are required for power up to 700 W, while powers higher than 1400 W cause cobalt to vaporize and, as a result, defects in the deposited track.

From this experiments, two setup configurations were identified in terms of laser power and irradiance (see Table 2), while powder feed rate (PFR) was kept constant and equal to 11.6 g/min. The process parameters of REF1 and REF2 allow for the production of a well-adhered deposit with low porosity (mean values of the track and maximum values of each analyzed section both less than 5 %). REF1 samples have finer WC particles than REF2 samples (Fig. 2), indicating that as laser power is increased, more WC particles melt and dissolve in the matrix, according to [15]. However, high power causes the low-melting metal to partially evaporate, increasing the occurrence of voids, which resulted in higher porosity detected in REF1 compared to REF2 (see Section 3.1).

Starting from REF1 and REF2 three re-melting approaches were used, based on literature evidence (approaches a, b) and in opposition with them (approach b), as follows (see also Table 3): (a) remelting power = REF power (RP) + 80 % (RP) and remelting speed = REF speed x 5 [26]; (b) as in approach "a", but dividing the calculated power and speed by a factor of 10; (c) remelting power = REF power (RP) - 50 % (RP) and remelting speed = REF speed (starting from results in [23]). Three repetitions were carried out for each set of process parameters and for the chosen approach repurposed by increasing the number of remelting passes from 1 to 4.

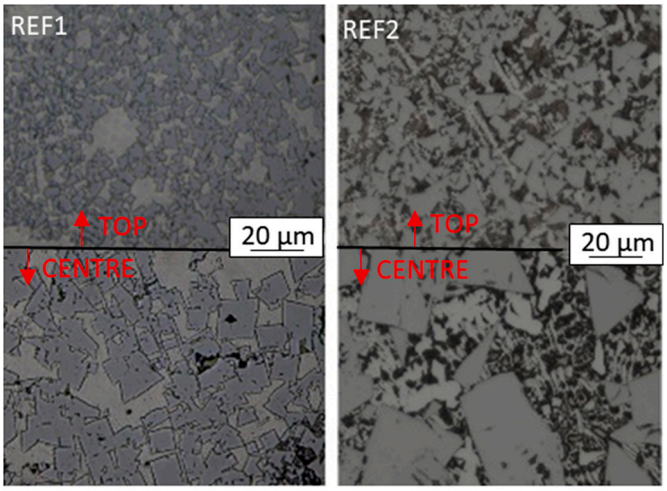

Fig. 2. Microstructure of REF1 (a) and REF2 (b) depositions observed through earlier research.

Table 3
Remelting process parameters for single track's deposition.

REF	Remelting approach	Power [W]	Scan speed [mm/s]	Irradiance [W/cm^2]
REF1	RM_1	2340	40	6.16×10^4
	RM_2	230	4	0.61×10^4
	RM_3	650	8	1.71×10^4
REF2	RM_1	1620	40	4.26×10^4
	RM_2	160	4	0.42×10^4
	RM_3	450	8	1.18×10^4

The process was replicated on multitrack samples after selecting the first deposit's process parameters, the best remelting approach, and the number of remeltings. In this configuration, the effect of the focal position during the remelting step (h_{REM}) was also analyzed by evaluating three levels: absence of defocus (spot 2.2 mm in diameter), defocus of 0.6 mm and 1.2 mm (defocus spot ≈2.3 mm in diameter, with consequent Irradiance reduction of ≈10 %). The defocus was set at a height of +35 % (focal plane under the surface) and + 130 % (focal plane above the surface) of the initial base plate (see Fig. 1c), taking into account the measured height of the first deposited track (0.93 ± 0.18 mm). Finally, for the last stage (multitrack and multilayer configuration) also the focal plane position for the second layer (h_{2D}) deposition was considered and varied: +0.6 mm, +1 mm and +1.2 mm respect to the base plane.

2.2. Deposited tracks and layers analysis

Metallographic samples were prepared by cutting the samples in the middle of the track by EDM and polishing the resulting surface by using Aka polishing method for hard metals: disk with grit from 125 µm to 75 µm using water as cooler and lubricant, then disks from 9 to 1 µm with diamond paste as lubricant.

The specimens were preliminary analyzed after polishing for defects evaluation, then etched with a Murakami chemical etchant with a swab time of 10 s for microstructure evaluation. The deposited tracks and layers were examined using optical microscopy (OM, Nikon Optiphot-100), and average porosity was calculated using ImageJ free software. More in-depth microstructural analysis was then performed using a SEM-FEG microscope (Tescan Mira3 with Schottky emitter), and the chemical composition was evaluated by an EDS probe (Bruker X-Flash 630 M) for micro elemental analysis.

Following microstructural analysis, Vickers microhardness tests were performed using a micro-durometer (HX-1000, Remet) with 1 kg load (HV1) and a dwell time of 15 s. In-depth indentations were made in the middle of the melted and resolidified area, with a space between each indentation of ≈170 µm, starting from ≈100 µm from the surface. In case of multitrack and multilayer samples also longitudinal indentation were made inside each layer and in the bonding region between them for evaluating the effect of subsequent deposition on final hardness. The distance between each indentation was ≈160 µm.

3. Results and discussion

3.1. Single track

Single-track samples were produced in accordance with the parameters described in Table 3 and Fig. 3 illustrates the outcomes of one of the three repetitions as an example. The analyses carried out by OM have the following features from a microstructural perspective:

- With the exception of the RM_1 case, which results in a slight flattening of the track, none of the methods used for remelting the deposited layer appear to make any obvious changes starting with the REF2 parameters.
- The track flattens noticeably also when using the RM_1 method and REF1 process parameters, highlighting the effects of power on track morphology.
- The metallurgical structure of the deposit is altered by the combination of the REF1 parameters and the RM_3 remelting strategy, highlighting a superficial white layer.

Image analysis was done on each sample in regards to the resulting porosity, and the mean values with standard deviation are displayed in Fig. 4 for each setup. When using REF1 and REF2 as the reference parameters, as-cladded samples show mean porosities of 3.8 % and 1.3 %, respectively. These percentages drop in both cases when the RM_3

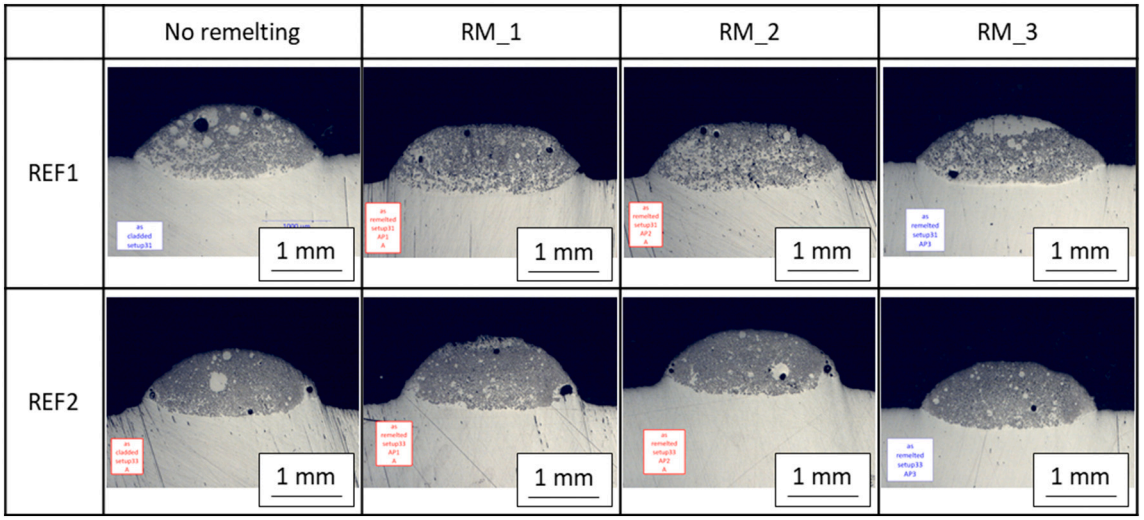

Fig. 3. OM images of single-track tests in the as-cladded state and after one remelting passage using different remelting strategies.

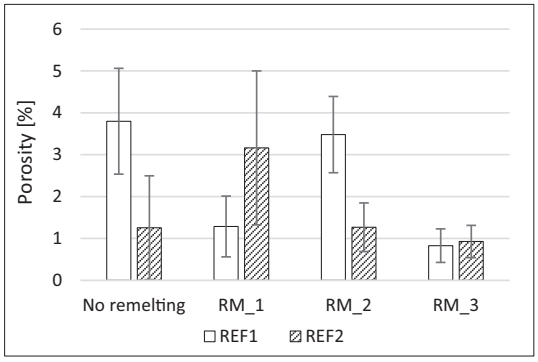

Fig. 4. Measured porosity for as-cladded and remelted samples.

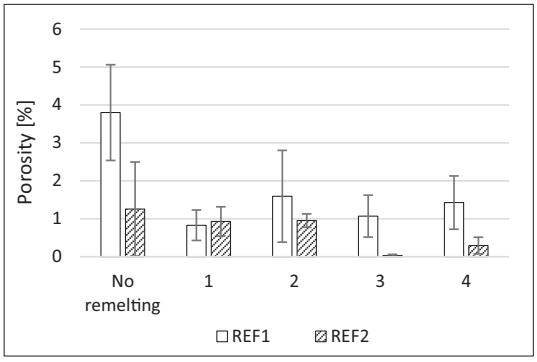

Fig. 6. Measured porosity at number of remelting crossings increasing.

remelting approach is added, taking on values of 0.8 % for REF1 and 0.9 % for REF2, demonstrating the benefit of using moderate power for the remelting method. A clarification is required for the REF1 sample after RM_1: a high porosity was detected in one of the evaluated samples due to the presence of some large pores. As a result, this value had a significant impact on the final mean density. However, no evidence led to the conclusion that remelting played a role in this specific outcome.

RM_3 was thus used for evaluating the effects of subsequent remelting steps from 1 to 4 and the results are shown in Fig. 5 and Fig. 6 respectively for microstructure and porosities evaluations.

These findings suggest that the effect of remelting is significantly influenced by the process parameters defined for deposition. Starting with REF1, the subsequent remelting has an impact on both the microstructure, confirming the existence of a white superficial layer even

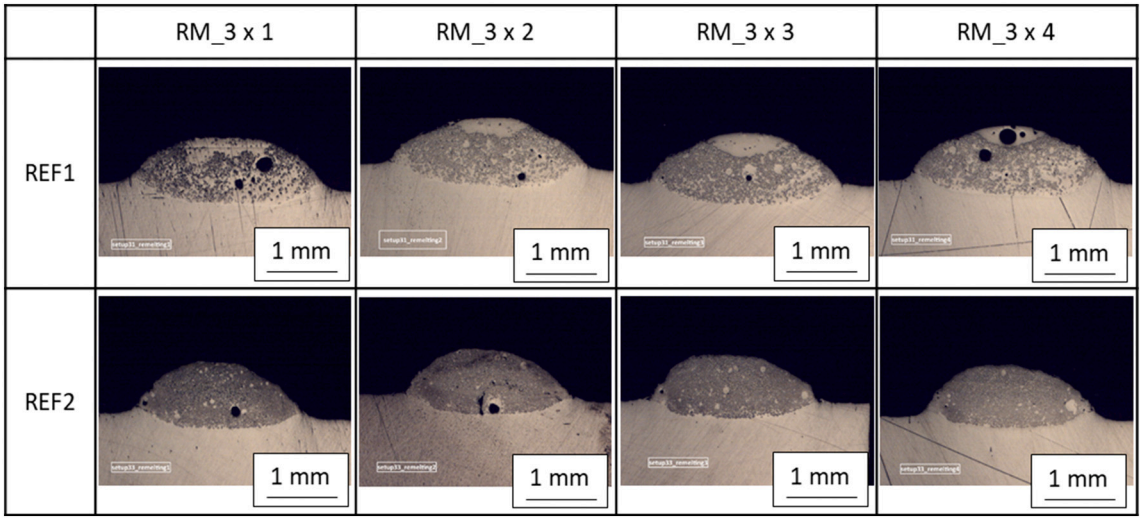

Fig. 5. OM images of single-track tests after increasing number of remelting crossings.

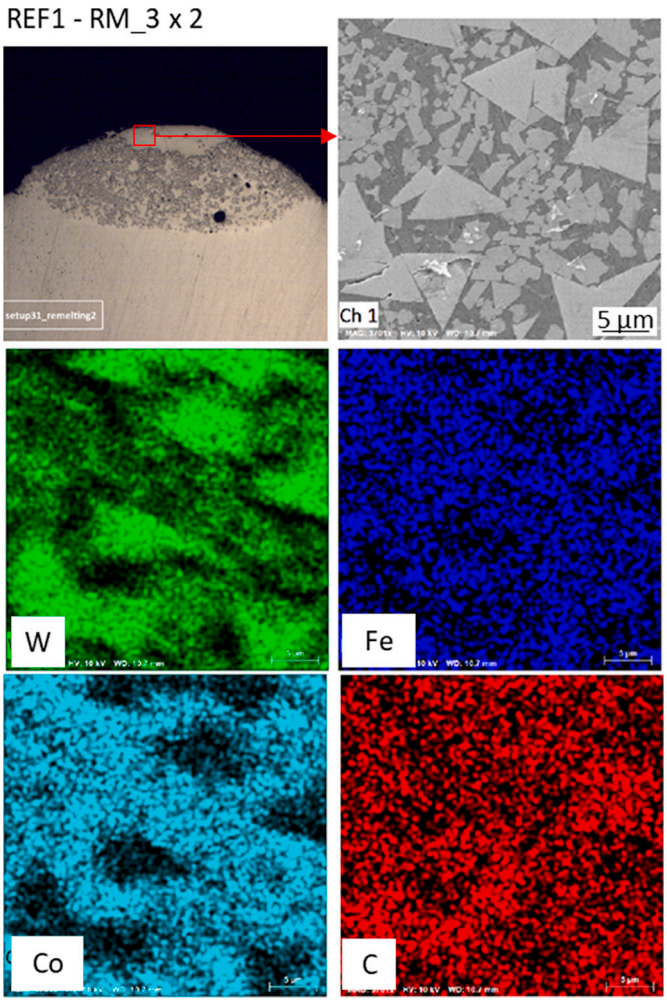

Fig. 7. White layer composition highlighted by SEM-EDS analysis.

when the number of passes varies, and the porosity, which significantly decreases in comparison to the as-cladded condition. SEM and EDS micro-elemental analysis were used to observe this surface modification. As shown in Fig. 7, WC-Co particles with sizes ranging from 3 to 7 µm (detailed analysis will be presented in the following sections) are surrounded by a (Fe-Co-C)-rich matrix inside the white layer.

Remelting's influence becomes less obvious when starting with the REF2 parameters. Although the initial porosity was lower than in the cladded state, after remelting there was no sign of a white layer or altered microstructure. The REF2 process parameters were left out of the subsequent experimental campaign under the assumption that any potential improvement in the adhesion of the second layer results from a change in the first layer's surface chemical composition after remelting.

Regarding the ideal number of remelting passes, it can be seen that the white surface starts to appear even after the first pass and that the effect on densities is always noticeable without significant variations.

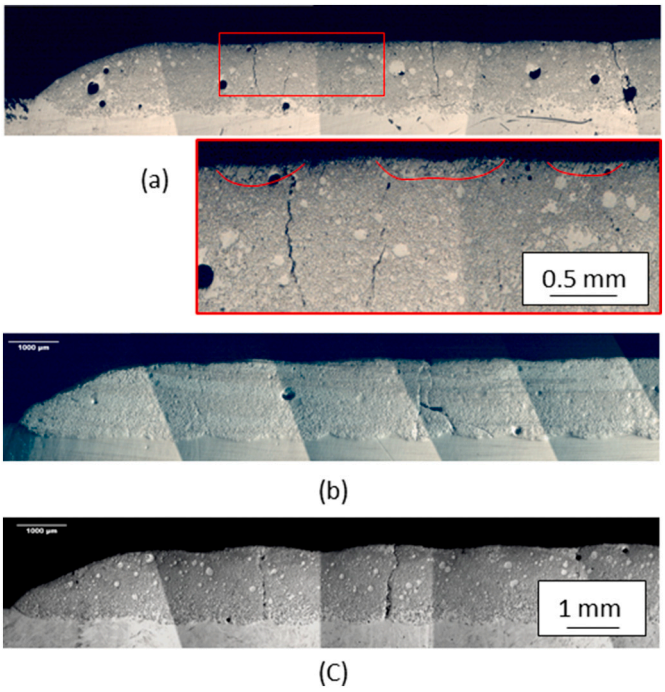

Fig. 9. Effect of remelting focal plane position respect to the base plate: h_{REM} = 0 mm (a), h_{REM} = 0.6 mm (b), h_{REM} = 1.2 mm (c).

3.2. Single layer

For the single track, the RM_3 remelting approach and the REF1 reference parameters were defined, and some additional tests were run to determine the impact of remelting under multitrack circumstances. Twelve adjacent tracks that were placed next to one another and spaced 1.3 mm were used to build these layers. Fig. 8 compares a multitrack sample without remelting (8a) to one that has been remelted (8b). This initial comparison allows for the identification of three key features:

- The formation of cracks that were not present during the deposition of the single track is highlighted in the production of WC-Co layers (the most important are marked with red arrows in Fig. 8), both in as-cladded and re-melted configuration.
- The addition of remelting ensures that the layer's surface is more uniform and less wavy at the end of the process.
- As additional tracks are deposited, the dilution of the material with the substrate remains constant.

Fig. 9 reports the findings with regard to the impact of focal plane position during remelting: while any notable difference is highlighted between h_{REM} = 0 mm and h_{REM} = 0.6 mm, a focal plane above the surface of the first deposited layer prevents uniformizing the surface. Again, for following tests of the second layer's deposition, both conditions were preserved.

A further point that must be mentioned is that, even when the same process parameters are used for the deposition of the material in multitrack samples, the “white layer” effect of remelting is much less

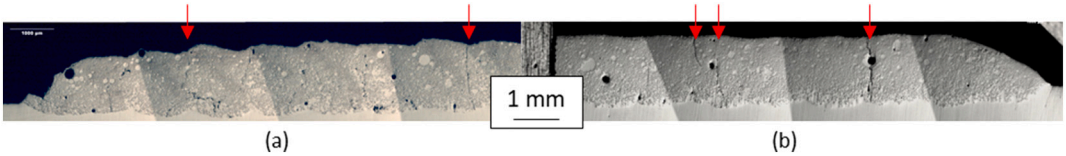

Fig. 8. OM of as-cladded (a) and remelted (b) multitrack samples. Transversal main cracks are highlighted with red arrows in both samples. (For interpretation of the references to colour in this figure legend, the reader is referred to the web version of this article.)

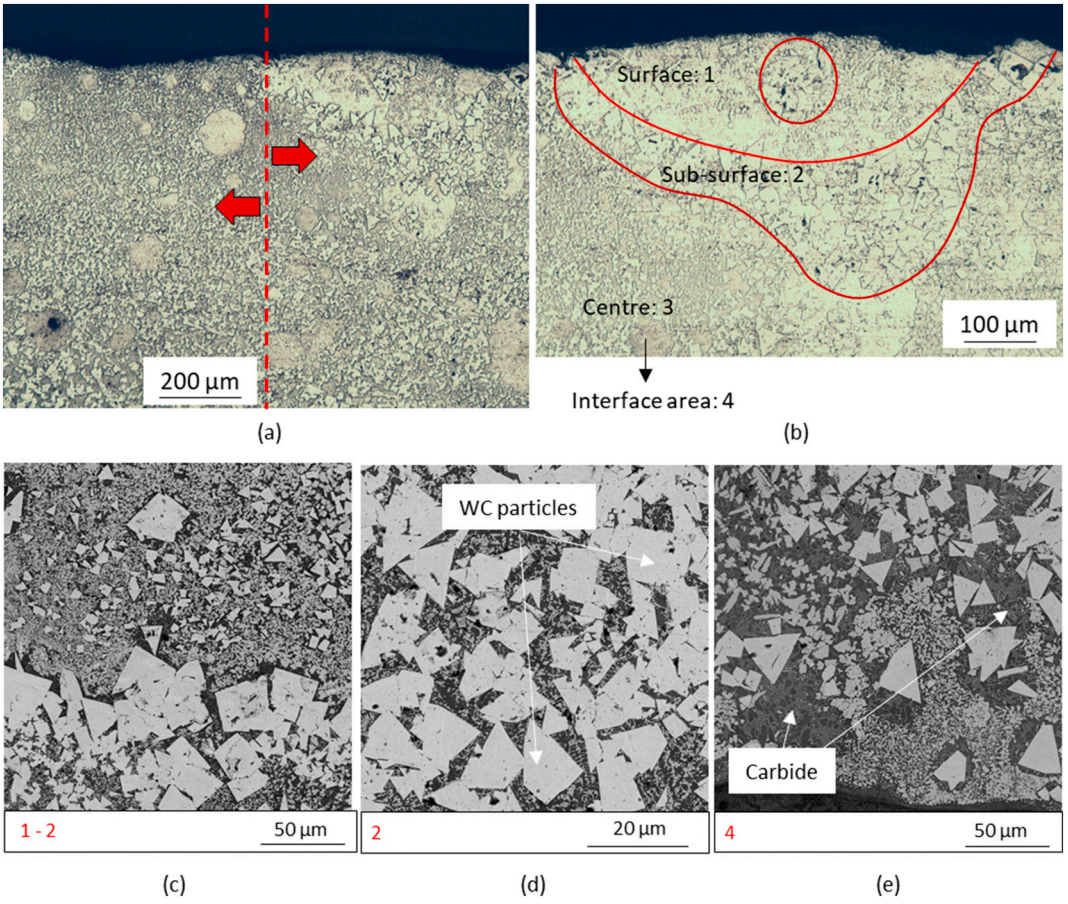

Fig. 10. OM (a,b) and SEM (c,d,e) microstructure analysis of deposited and remelted samples. SEM images shows the microstructure of three main region of interest described in (a,b): surface (c), sub-surface (d) and deposit/substrate interface (e).

noticeable. In fact, looking at the enlargement at the side of Fig. 9a that this area is tiny and acts as a trigger point for cracks.

In depth microstructure analysis, performed on the same sample depicted in Fig. 9a, show the effects of the DED-based cladding process and subsequent remelting on size, distribution and morphology of particles and compounds across main areas of interest of the deposited material, as can be observed in Fig. 10. First, Fig. 10a shows at lower magnification a region of the layer with no remelting effect (left), which corresponds to a region not directly impacted by the laser-deposit interaction during remelting, and a region with a remelting effect that is clearly visible (right). Fig. 10b enlarges this second area and separates it into four distinct areas of interest: superficial "white layer" region (1), sub-superficial region (2), center (3) and interface region (4; not visible). SEM micrograph are then reported to better show the microstructure of these relevant areas. The superficial region, directly affected by remelting effects, (Fig. 10c) presents evenly distributed WC particles that, on average, are less than 8 µm in size, submerged in a (Co-Fe-C)-rich matrix and it is followed by a sub-surface zone with much larger WC particles, with elements reaching 20 µm in size (Fig. 10c, d). Convective flows could enable larger WC particles sink to the bottom of the melt pool, leaving smaller WC-Co and metal matrix at the surface due to density differences, which is a possible explanation for the formation of white layers after remelting, when only a superficial portion of the deposited material melts again. Chong et al. [27] described the same phenomenon in order to explain the different distributions of WC particles in the clad layer. This would also explain why this effect only appears for the RM_3 parameters. High power and low speed are favorable for the convective flux of melted material, but in RM_1, the speed is too high and the power is high enough to vaporize a small amount of the deposited surface. The power in RM_2, on the other hand,

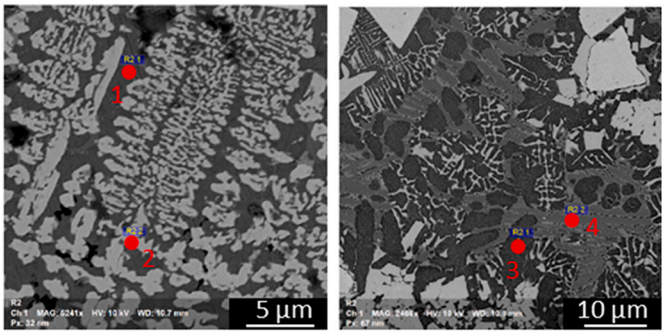

Chemical composition [wt. %]

Spectrum	C	O	Fe	Co	W
1	9.1	/	61.0	23.5	6.1
2	8.5	1.2	21.1	9.0	60.2
3	6.3	2.5	75.6	6.5	9.0
4	7.8	/	69.8	6.4	16.0

Fig. 11. Microanalyses performed in order to determine the chemical composition of the identified complex carbide.

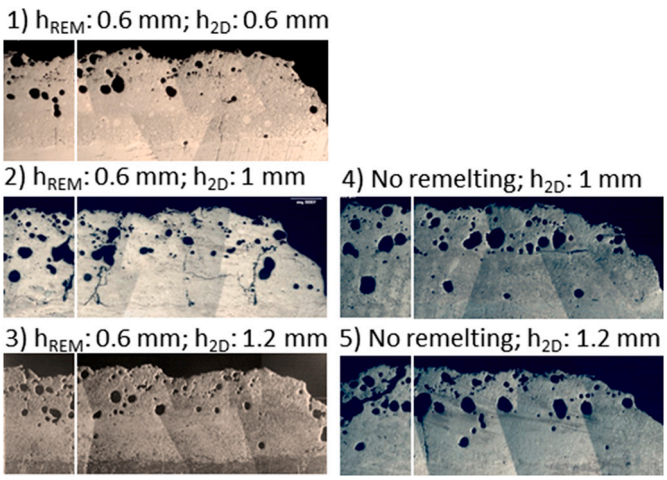

Fig. 12. Laser remelting effect on 2nd layer deposition of WC-Co.

Table 4
Porosity and hardness of WC-Co multilayer using re-melting strategy between the two depositions.

Sample	Porosity [%]	Mean hardness [HRC] 1st layer	Mean hardness [HRC] 2nd layer
1	5.85	72.9 ± 1.18	74.1 ± 1.3
2	6.13		
3	4.22		
4	8.96		
5	10.30		

is probably insufficient to remelt the deposited material.

Homogeneity in WC particles distribution vanishes as we get closer to the interface zone (Fig. 10e), the WC particle sizes vary, and the matrix becomes complex and rich in columnar carbides and complex eutectic carbides, as shown in Fig. 11 and well explained by several authors [15,28]. The steel alloying elements of the substrate and the slower cooling rates, in fact, promote abundant precipitation of carbides across the cladding/substrate interface as a result of WC particles melting and dissolving in the matrix.

Finally, when the remelting parameters and the number of remelting varied, no significant average difference was found in the hardness of the deposited layers. Measured average values and standard deviations of the deposit's hardness are respectively: 75.4 HRC, 2.94.

3.3. Multilayer

Previous results have demonstrated that a remelting step affects the microstructure and the flatness of the deposit in the single-track setup and on the layer. The method was tested with this onset in the deposition of a second layer. The primary samples are displayed in Fig. 12. Each specimen's microstructure is displayed at the start of the path and in a representative section in the middle of the path. Table 4 provides additional information about the obtained results, including the deposits' porosity and the average hardness determined on the first and second layer.

The deposition of a second layer is still crucial due to the mechanical and thermal properties of the first WC-Co layer, as can be seen from an analysis of the images and the results in terms of porosity. The addition of remelting, in fact, does not allow obtaining layers of considerable size without defects. However, it should be noted that the porosity reduction is not negligible and it allows for a reduction in defects from 10.3 % to 4.2 % using the same process parameters. This decrease in porosity affects both the porosities that exist after the first layer and those that are formed during the second layer's deposition. In conclusion, by reducing waviness and forming white layers, remelting improves the quality of the second layer. A smoother surface produced a layer that was less convex and, as a result, had higher absorptivity, while a concentration of low-melting elements on the surface improves the dilution of the second layer with the first. Thermal dissipation brought on by stronger layer bonding is likely the main factor reducing porosity.

In addition to laser remelting, the focal plane position that was used for the second layer's deposition appears to be significant. A specific experimental campaign would be required to determine whether this behavior is repeatable, but a focal plane just above or below the first deposit surface seems to prevent cracks from propagating.

In terms of hardness, the average hardness of the upper layer is lower if compared to the case of a single deposit (which was equal to 75.4 HRC), and there is even less hardness between the layer that is most superficial and the layer that adheres to the steel substrate.

4. Conclusion

The medium-large area multilayer deposition of WC-Co on a steel substrate is a challenging process because each subsequent layer relies on the heat dissipation and dilution properties of the preceding hard metal layer. This results in the development of porosity and cracks, which may affect the deposit's mechanical and tribological properties. To address this criticality, the following work proposes to take advantage of the recognized benefits of first-layer remelting before proceeding with second-layer deposition. The proposed methodology began with a single trace and progressed to investigate the remelting effects on single and double layers. Process conditions under which remelting modifies the structure of a deposit's surface layer have been established by carefully analyzing the deposit and remelting process parameters. The most relevant results of the work can be summarized as follows:

- In a single-track configuration, when using the optimum remelting approach (moderate power for the remelting strategy), the porosity percentage drops to less than 1 %, representing a 75 % reduction over the as-cladded condition.
- In single-layer configuration: remelting ensures that the layer's surface is more smooth and less wavy at the end of the process, but cracks form in both the as-cladded and re-melted configurations.
- In multilayer configuration: Despite the fact that the deposit's residual porosity remains high (4–6 %), the formation of this white layer has proven to be beneficial for the deposition of subsequent layers, reducing porosity by 60 %.
- In all cases, the SEM analysis of the microstructurally-modified surface layer, which appears white under the optical microscope, revealed a matrix rich in Fe, Co, and C elements with small WC particles (8 μm) homogeneously dispersed within it.

CRediT authorship contribution statement

Erica Liverani: Conceptualization, Writing – original draft. **Alessandro Ascari:** Methodology, Investigation. **Alessandro Fortunato:** Validation, Writing – review & editing.

Declaration of competing interest

The authors declare that they have no known competing financial interests or personal relationships that could have appeared to influence the work reported in this paper.

Data availability

Data will be made available on request.

References

[1] D. Svetlizky, B. Zheng, A. Vyatskikh, M. Das, S. Bose, A. Bandyopadhyay, J. M. Schoenung, E.J. Lavernia, N. Eliaz, Laser-based directed energy deposition (DED-LB) of advanced materials, Mater. Sci. Eng. A 840 (2022), 142967, https://doi.org/10.1016/j.msea.2022.142967.

[2] M. Zhong, W. Liu, Laser surface cladding: the state of the art and challenges, Proc. Inst. Mech. Eng. C J. Mech. Eng. Sci. 224 (5) (2010) 1041–1060, https://doi.org/10.1243/09544062JMES1782.

[3] J.M. Pappas, E.C. Kinzel, X. Dong, Laser direct deposited transparent magnesium aluminate spinel ceramics, Manuf. Lett. 24 (2020) 92–95, https://doi.org/10.1016/j.mfglet.2020.04.003.

[4] Y. Li, Y. Hu, W. Cong, L. Zhi, Z. Guo, Additive manufacturing of alumina using laser engineered net shaping: effects of deposition variables, Ceram. Int. 43 (2017) 7768–7775, https://doi.org/10.1016/j.ceramint.2017.03.085.

[5] S. Liu, Y.C. Shin, The influences of melting degree of TiC reinforcements on microstructure and mechanical properties of laser direct deposited Ti6Al4V-TiC composites, Mater. Des. 136 (2017) 185–195, https://doi.org/10.1016/j.matdes.2017.09.063.

[6] J. Wang, L. Li, C. Tan, H. Liu, P. Lin, Microstructure and tensile properties of TiCp/Ti6Al4V titanium matrix composites manufactured by laser melting deposition, J. Mater. Process. Technol. 252 (2018) 524–536, https://doi.org/10.1016/j.jmatprotec.2017.10.005.

[7] D. Svetlizky, M. Das, B. Zheng, A.L. Vyatskikh, S. Bose, A. Bandyopadhyay, J. M. Schoenung, E.J. Lavernia, N. Eliaz, Directed energy deposition (DED) additive manufacturing: physical characteristics, defects, challenges and applications, Mater. Today 49 (2021) 271–295, https://doi.org/10.1016/j.mattod.2021.03.020.

[8] H. Wang, W. Liu, Z. Tang, Y. Wang, X. Mei, K.M. Saleheen, Z. Wang, H. Zhang, Review on adaptive control of laser-directed energy deposition, Opt. Eng. 59 (2020) 70901, https://doi.org/10.1117/1.OE.59.7.070901.

[9] R.T. Jardin, V. Tuninetti, J.T. Tchuindjang, N. Hashemi, R. Carrus, A. Mertens, L. Duchene, H.S. Tran, A.M. Habraken, Sensitivity analysis in the modeling of a high-speed, steel, thin wall produced by directed energy deposition, Metals 10 (2010) 1554, https://doi.org/10.3390/met10111554.

[10] Q. Yang, P. Zhang, L. Cheng, Z. Min, M. Chyu, A.M. To, Finite element modeling and validation of thermomechanical behavior of Ti-6Al-4V in directed energy deposition additive manufacturing, Addit. Manuf. 12 (2016) 169–177, https://doi.org/10.1016/j.addma.2016.06.012.

[11] Y. Zhang, Y.K. Chen, D.S. Yu, D.Q. Sun, H.M. Li, A review paper on effect of the welding process of ceramics and metals, J. Mater. Res. Technol. 9 (6) (2020) 16214–16236, https://doi.org/10.1016/j.jmrt.2020.11.088.

[12] S. Zhou, X. Zeng, Q. Hu, Y. Huang, Analysis of crack behavior for ni-based WC composite coatings by laser cladding and crack-free realization, Appl. Surf. Sci. 255 (5) (2008) 1646–1653, https://doi.org/10.1016/j.apsusc.2008.04.003.

[13] D.D. Liu, Y. Chen, L. Li, F. Li, In situ investigation of fracture behavior in monocrystalline WCp-reinforced Ti–6Al–4V metal matrix composites produced by laser melt injection, Scr. Mater. 59 (1) (2008) 91–94, https://doi.org/10.1016/j.scriptamat.2008.02.033.

[14] X. Shen, X. He, L. Gao, G. Su, C. Xu, N. Xu, Study on crack behavior of laser cladding ceramic-metal composite coating with high content of WC, Ceram. Int. 48 (12) (2022) 17460–17470, https://doi.org/10.1016/j.ceramint.2022.03.010.

[15] C. Jiang, J. Zhang, Y. Chen, Z. Hou, Q. Zhao, Y. Li, L. Zhu, F. Zhang, Y. Zhao, On enhancing wear resistance of titanium alloys by laser cladded WC-co composite coatings, Int. J. Refract. Met. Hard Mater. 107 (2022), https://doi.org/10.1016/j.ijrmhm.2022.105902.

[16] Y. Liu, R. Sun, W. Niu, T. Zhang, Y. Lei, Effects of CeO_2 on microstructure and properties of TiC/Ti 2 Ni reinforced Ti-based laser cladding composite coatings, Opt. Lasers Eng. 120 (2019) 84–94. OI10.1016/j.optlaseng.2019.03.001.

[17] T. Perrin, S. Achache, P.J. Meausoone, F. Sanchette, Characterization of WC-doped NiCrBSi coatings deposited by laser cladding; effects of particle size and content of WC powder, Surf. Coat. Technol. 425 (2021), 127703, https://doi.org/10.1016/j.surfcoat.2021.127703.

[18] A. Sadhu, A. Choudhary, S. Sarkar, A.M. Nair, P. Nayak, S. Dadasahed Pawar, G. Muvvala, S.K. Pal, A.K. Nath, A study on the influence of substrate pre-heating on mitigation of cracks in direct metal laser deposition of NiCrSiBC-60%WC ceramic coating on inconel 718, Surf. Coat. Technol. 389 (2020), 125646, https://doi.org/10.1016/j.surfcoat.2020.125646.

[19] Y. Xiong, J.E. Smugeresky, L. Ajdelsztajn, J.M. Schoenung, Fabrication of WC–Co cermets by laser engineered net shaping, Mater. Sci. Eng. A 493 (2008) 261–266, https://doi.org/10.1016/j.msea.2007.05.125.

[20] V.K. Balla, S. Bose, A. Bandyopadhyay, Microstructure and wear properties of laser deposited WC–12%Co composites, Mater. Sci. Eng. A 527 (2010) 6677–6682, https://doi.org/10.1016/j.msea.2010.07.006.

[21] W. Wang, S. Zhang, S. Xiao, Y.S. Sato, D. Wang, Y. Liu, D. Liu, Q. Hu, Microstructure and properties of multilayer WC-40Co coating on ti-6Al-4V by electron beam cladding, Mater. Charact. 183 (2022), 111585, https://doi.org/10.1016/j.matchar.2021.111585.

[22] Q. Wang, Q. Li, L. Zhang, D.X. Chen, H. Jin, J. Dong Li, J. Wei Zhang, C. Yan Ban, Microstructure and properties of ni-WC gradient composite coating prepared by laser cladding, Ceram. Int. 48 (6) (2022) 7905–7917, https://doi.org/10.1016/j.ceramint.2021.11.338.

[23] Z. Yu, Y. Zheng, J. Chen, C. Wu, J. Xu, H. Lu, C. Yu, Effect of laser remelting processing on microstructure and mechanical properties of 17–4 PH stainless steel during laser direct metal deposition, J. Mater. Process. Technol. 284 (2020), 116738, https://doi.org/10.1016/j.jmatprotec.2020.116738.

[24] J. Mateos, J.M. Cuetos, E. Fernández, R. Vijande, Tribological behaviour of plasma-sprayed WC coatings with and without laser remelting, Wear 239 (2000) 274–281, https://doi.org/10.1016/S0043-1648(00)00325-2.

[25] M. Afzal, M. Ajmal, A. Nusair Khan, T.I. Khan, T. Ben Mahmud, Effect of laser melting on plasma sprayed WC-12 wt.%Co coatings, Surf. Coat. Technol. 266 (2015) 22–30, https://doi.org/10.1016/j.surfcoat.2015.02.004.

[26] S. Zhou, Y. Xu, B. Liao, Y. Sun, X. Dai, J. Yang, Z. Li, Effect of laser remelting on microstructure and properties of WC reinforced fe-based amorphous composite coatings by laser cladding, Opt. Laser Technol. 103 (2018) 8–16, https://doi.org/10.1016/j.optlastec.2018.01.024.

[27] P.H. Chong, H.C. Man, T.M. Yue, Microstructure and wear properties of laser surface-cladded Mo–WC MMC on AA6061 aluminum alloy, Surf. Coat. Technol. 145 (2001) 51–59, https://doi.org/10.1016/S0257-8972(01)01286-5.

[28] M. Hu, J.C. Tang, X.G. Chen, N. Ye, X.Y. Zhao, M.M. Xu, Microstructure and properties of WC-12Co composite coatings prepared by laser cladding, Trans. Nonferrous Metals Soc. China 30 (4) (2020) 1017–1030, https://doi.org/10.1016/S1003-6326(20)65273-6.